Earth Planets Space, **63**, 57–69, 2011

Improvement in the accuracy of expected seismic intensities for earthquake early warning in Japan using empirically estimated site amplification factors

Kazuhiro Iwakiri[1], Mitsuyuki Hoshiba[1], Kouji Nakamura[2], and Nobuyuki Morikawa[3]

[1]*Meteorological Research Institute, Nagamine 1-1, Tsukuba 305-0031, Japan*
[2]*Japan Meteorological Agency, Ohte-machi 1-3-4, Chiyoda, Tokyo 100-8122, Japan*
[3]*National Research Institute for Earth Science and Disaster Prevention, Tennodai, Tsukuba 305-0006, Japan*

(Received April 12, 2010; Revised December 8, 2010; Accepted December 10, 2010; Online published February 28, 2011)

The Japan Meteorological Agency (JMA) is able to process data for its earthquake early warning (EEW) procedure very quickly by employing a seismic intensity expectation method that uses simplified strong motion characteristics. To represent one of these characteristics, the site amplification factor at the seismic intensity station, JMA uses ARV (amplitude ratio of peak ground velocity at the ground surface relative to the engineering bedrock of average S-wave velocity 700 m/s) based on topographic data. As a potential substitute for the ARV, we investigated a station correction based on empirical site amplifications obtained from recent observed seismic intensity data. When estimating this station correction, we removed an effect of the abnormal seismic intensity distribution of deep subduction-zone earthquakes and applied a correction for the earthquake source term to the attenuation relation. Station corrections were obtained for 1258 stations, representing about 30% of all current seismic intensity stations. The correlation between our station corrections at the stations and the site amplification based on topographic data is weak (correlation coefficient = 0.30). The error of the expected seismic intensity was improved by 15% by replacing ARV with the station correction.

Key words: Earthquake early warning, seismic intensity expectation, site amplification factor, attenuation relation.

1. Introduction

Observed strong motion characteristics of earthquakes generally consist of source effects, wave propagation path effects, and site effects (e.g., Iwata and Irikura, 1986). For accurate evaluation of strong motion taking into account these effects, an understanding of the fault rupture process, the attenuation structure of seismic waves and, especially, the local soil conditions is indispensible. Strong motion varies greatly and depends on the degree of amplification by the subsurface ground structure, even for events of the same magnitude and with the same seismic wave propagation paths.

The Japan Meteorological Agency (JMA) began providing earthquake early warning (EEW) services to the general public on 1 October 2007 with the aim of mitigating seismic disasters (Hoshiba *et al*., 2008; Kamigaichi *et al*., 2009; Doi, 2010). An EEW notification includes information on the expectation of strong ground motion immediately after an earthquake, but before destructive strong motion arrives, by processing real-time data obtained at one or a few seismometers positioned near the source region. To achieve such rapid processing, the JMA employs an expectation method that uses three major factors controlling strong motion: (1) the earthquake magnitude M estimated from P-wave amplitude to represent source effects; (2) the attenuation relation to model wave propagation path effects; (3) a site amplification factor, ARV (amplitude ratio of peak ground velocity at the ground surface relative to the engineering bedrock of average S-wave velocity 700 m/s) for site effects.

The technique for quick determination of the hypocenter and M in the JMA EEW uses waveform data collected from about 200 accelerometers of the JMA seismometer network (Harada, 2007) and from about 800 high-gain seismometers (velocity-type sensor; natural period is 1 s) of the Hi-net network of the National Research Institute for Earth Science and Disaster Prevention (NIED) (Okada *et al*., 2004). Strong motion intensity expectation in the JMA EEW is performed on seismic intensity measurements on the JMA scale. The expectation of seismic intensity is based on the empirical methods of Si and Midorikawa (1999), Matsuoka and Midorikawa (1994), and Midorikawa *et al*. (1999), which are based on the hypocentral distance, focal depth, M, and site amplification factor.

The instrumental observation of seismic intensity started in 1990s in Japan. The first seismic intensity meters were installed in 1991, and their function was enhanced in 1996 (JMA, 1996). In addition, local governments and NIED started to install seismic intensity meters in 1996. At the present time, at least one seismic intensity meter is installed at each village, town, ward, and

doi:10.5047/eps.2010.12.002

city in Japan. These meters are relatively densely deployed in populated areas and sparsely at mountain areas and there are currently about 4,200 stations throughout Japan (JMA, 2009; JMA, http://www.seisvol.kishou.go.jp/eq/intens_st/index.html). The data on instrumental seismic intensity is compiled by JMA according to the method explained on the JMA website (http://www.seisvol.kishou.go.jp/eq/kyoshin/kaisetsu/calc_sindo.htm), the Headquarters for Earthquake Research Promotion website (http://www.hp1039.jishin.go.jp/eqchreng/at2-4.htm), and Hoshiba *et al*. (2010). The observed seismic intensity at each station provides information that helps determine the initial response to disasters immediately after an earthquake. For example, when the observed instrumental seismic intensity is $\geq$5.5 on the JMA scale, an emergency assembly team conference is held at the Prime Minister's office.

There are two categories in the JMA EEW notification, namely, "warning" and "forecast". Japan is divided into 187 regions depending on prefectural borders, and the category of "warning" or "forecast" is issued on a per-region basis (Doi, 2010). Between two and 95 seismic intensity meters have been installed in each region. The seismic intensity is expected at the locations of the intensity meters, and the category of "warning" or "forecast" is issued depending on the expected intensities. When the expectation at one or more stations is $\geq$2.5 on the JMA scale (or M is estimated to be $>$3.5), a "forecast" is issued for the region; when it is $\geq$4.5, a "warning" is issued (Hoshiba *et al*., 2008). Note that, under the current operating conditions of the JMA EEW, the expectation of seismic intensity is performed for those locations where seismic intensity meters are installed (and not for whole area, including the locations where intensity meters are not installed). The site amplification factor at the site is an important factor in the expectation of the intensity. In the current system, ARV estimated from topographic data (Matsuoka and Midorikawa, 1994) is used to represent the site factor. However, topographic information may not be the best way to obtain site amplification estimates at each station. Additionally, most seismic intensity stations do not collect enough information on local soil conditions, such as borehole logs in the upper engineering bedrock, for site amplification to be estimated.

In the study reported here, we explored the possibility of using a station correction factor at the seismic intensity station, namely, an empirical site amplification estimate derived from peak ground velocity converted from seismic intensities observed in recent years, instead of the site amplification factor ARV based on topographic data. A number of studies that a station correction were estimated from comparison of the observed seismic intensities and the expected values by the attenuation relation. Fujiwara *et al*. (2007) estimated the station correction based on seismic intensity using the attenuation relation of seismic intensity; the results showed a weak correlation between the station correction at the sites and the site amplification based on topographic data. Kiyomoto *et al*. (2010) used the attenuation relation of JMA EEW's logic to estimate station corrections; but only at 5% of all stations. Our overall aim is to improve the accuracy of the expected seismic intensity of JMA EEW at the locations where seismic intensity meters have been installed. We therefore used the attenuation relation of JMA EEW's logic to estimate station corrections and defined the station correction as the amplification factor of peak ground velocity, similarly to the ARV, in order to be able to directly apply it to JMA EEW's logic. As these station corrections are based on observed seismic data, they may improve the accuracy of seismic intensity expectation at the sites. We applied the station correction to expected seismic intensity and evaluated it as a replacement for ARV. All of the logarithms described herein are common logarithms.

2. Method for Estimation of Station Corrections

The EEW procedure of seismic intensity expectation consists of four steps (Hoshiba *et al*., 2008; JMA Seismological Volcanological Department, 2008; Kamigaichi *et al*., 2009).

Step 1. Hypocentral parameters (origin time, location, and M) are determined immediately after the detection of seismic waves at one or a few seismometers near the source region. M is estimated from P-wave amplitude of displacement data by the method of Aketagawa *et al*. (2010) and from the whole waveform by the method of Kiyomoto *et al*. (2010). These formulas were constructed using regression analysis of JMA magnitude, M_{j}, in the JMA seismic catalog. M_{j} is converted to moment magnitude M_{w} by the empirical relationship (Utsu, 1982)

$$M_{\mathrm{w}} = M_{\mathrm{j}} - 0.171. \tag{1}$$

Step 2. PGV600, peak ground velocity (cm/s) at the engineering bedrock with an average S-wave velocity of 600 m/s, is estimated from the attenuation relation by Si and Midorikawa (1999) as

$$\begin{aligned}\log(\mathrm{PGV600}) = {} & 0.58M_{\mathrm{w}} + 0.0038D + d \\ & - \log\left(X + 0.0028 \cdot 10^{0.5M_{\mathrm{w}}}\right) \\ & - 0.002X - 1.29,\end{aligned} \tag{2}$$

where D is focal depth (km), X is the shortest distance (km) to the ruptured fault (hereinafter referred as fault distance), and d is a coefficient that is 0.0 for inland crustal earthquakes, -0.02 for inter-plate earthquakes, and 0.12 for intra-slab earthquakes. This attenuation relation is widely used in Japan (e.g., Headquarters for Earthquake Research Promotion, 2009) as an empirical estimation method for strong ground motions. In this study, we use 0.0 for d for all earthquake types in EEW. For X, the fault model (location, length, width, strike, and dip angle) is unknown during EEW processing. Here, we assume (1) the progress of rupture to be bilateral from the center of the fault and (2) the fault geometry to be a circle with a radius of half of the rupture length from hypocenter. Thus $X = R - L/2$ is used for the fault distance, where R is hypocentral distance (km) and L is the rupture length (km) estimated by the empirical relation (Utsu, 2001)

$$\log L = 0.5M_{\mathrm{w}} - 1.85. \tag{3}$$

If R is shorter than $L/2$, X is fixed to be 3 km.

Table 1. Earthquakes whose fault distance was estimated from fault model.

No.	Date (y.m.d)	Source region	M_j	Focal depth (km)	Earthquake type	References of fault model
1	1996.10.19	Hyuganada	6.9	34	Inter-plate	Kikuchi (1996)*1
2	1997.03.26	NW Kagoshima Pref.	6.6	12	Crustal	Kikuchi and Yamanaka (1997a), Miyamachi *et al.* (1999)*1
3	1997.05.13	NW Kagoshima Pref.	6.4	9	Crustal	Kikuchi and Yamanaka (1997b), Miyamachi *et al.* (1999)*1
4	1997.06.25	Yamaguchi Pref.	6.6	8	Crustal	Kikuchi and Yamanaka (1997c)*1
5	1998.09.03	Northern Iwate Pref.	6.2	8	Crustal	Matsusaki *et al.* (2006)
6	2000.07.01	Near Niijima Island	6.5	16	Crustal	Matsusaki *et al.* (2006)
7	2000.07.09	Near Niijima Island	6.1	15	Crustal	Matsusaki *et al.* (2006)
8	2000.07.15	Near Niijima Island	6.3	10	Crustal	Matsusaki *et al.* (2006)
9	2000.07.30	Near Miyakejima Island	6.5	17	Crustal	Matsusaki *et al.* (2006)
10	2000.08.18	Near Niijima Island	6.1	12	Crustal	Matsusaki *et al.* (2006)
11	2000.10.06	Western Tottori Pref.	7.3	9	Crustal	GSI*2
12	2001.03.24	Akinada Setonaikai	6.7	46	Intra-plate	Matsusaki *et al.* (2006)
13	2003.05.26	Off Miyagi Pref.	7.1	72	Intra-plate	GSI*2
14	2003.07.26	Northern Miyagi Pref.	6.4	12	Crustal	GSI*2
15	2003.09.26	SE Off Tokachi	8.0	45	Inter-plate	GSI*2
16	2003.10.31	Off Fukushima Pref.	6.8	33	Inter-plate	Yamanaka (2003)
17	2004.10.23	Mid Niigata Pref.	6.8	13	Crustal	GSI*2
18	2004.10.27	Mid Niigata Pref.	6.1	12	Crustal	GSI*2
19	2004.11.08	Mid Niigata Pref.	5.9	0	Crustal	GSI*2
20	2004.11.29	Off Nemuro Peninsula	7.1	48	Inter-plate	GSI*2
21	2004.12.06	Off Nemuro Peninsula	6.9	46	Inter-plate	GSI*2
22	2004.12.14	Rumoi	6.1	9	Crustal	GSI*2
23	2005.03.20	NW Off Fukuoka Pref.	7.0	9	Crustal	GSI*2
24	2005.08.16	E Off Miyagi Pref.	7.2	42	Inter-plate	GSI*2
25	2007.03.25	Off Noto Peninsula	6.9	11	Crustal	GSI*2
26	2007.07.16	Off S Niigata Pref.	6.8	17	Crustal	GSI*2,*3
27	2008.05.08	Far E Off Ibaraki Pref.	7.0	51	Inter-plate	GSI*2
28	2008.06.14	Southern Iwate Pref.	7.2	8	Crustal	GSI*2
29	2008.07.24	Northern Iwate Pref.	6.8	108	Intra-plate	NIED (2008)

*1Location of fault model was read from aftershock distribution.
*2GSI: Geospatial Information Authority of Japan (http://www.gsi.go.jp/cais/HENDOU-hendou.html)
*3Southeast dip fault model was adopted.

Step 3. A site effect amplification factor ARV is estimated from AVS, the average S-wave velocity (m/s) of the subsurface structure down to a depth of 30 m, by

$$\log(\mathrm{ARV}) = 1.83 - 0.66\log(\mathrm{AVS}) \pm 0.16, \quad (4)$$

and AVS is empirically estimated using 1-km mesh topographic data (Matsuoka and Midorikawa, 1994). Because ARV defined in the JMA EEW is an amplification factor relative to PGV700 (peak ground velocity at the engineering bedrock of average S-wave velocity 700 m/s), PGV600 obtained from Eq. (2) is converted into PGV700 by multiplying it by 0.9 (JMA Seismological Volcanological Department, 2008). Thus, PGV at the free surface is estimated by

$$\mathrm{PGV} = \mathrm{PGV700} \times \mathrm{ARV}\ (= \mathrm{PGV600} \times 0.9 \times \mathrm{ARV}). \quad (5)$$

Step 4. Seismic intensity I (measured on the JMA intensity scale) at the ground surface is converted from peak ground velocity PGV by the empirical relation (Midorikawa *et al.*, 1999)

$$I = 2.68 + 1.72\log(\mathrm{PGV}) \pm 0.21. \quad (6)$$

This four-step procedure is the current JMA method for determining seismic intensity expectation for the EEW. In an attempt to improve this method, we replaced the ARV estimated using topographic data with a station correction, SC_j, estimated from observed seismic intensity for the j-th seismic intensity station by

$$\log\left(\mathrm{SC}_j\right) = \frac{1}{N_j}\sum^{N_j}\log\left(\mathrm{PGV}_{ij}^{\mathrm{obs}}/\mathrm{PGV700}_{ij}^{\mathrm{exp}}\right), \quad (7)$$

where N_j is the number of earthquakes observed at the j-th station. $\mathrm{PGV}_{ij}^{\mathrm{obs}}$ is the peak ground velocity converted from the observed seismic intensity using Eq. (6) for the i-th earthquake at the j-th station. $\mathrm{PGV700}_{ij}^{\mathrm{exp}}$ is estimated by an attenuation relation in which coefficient d is 0.0 in Eq. (2) (from Steps 2 and 3), and PGV700 = PGV600 × 0.9. For all subsequent discussion in this paper, "ARV" refers to the amplification factor estimated from topographic data, and "station correction" refers to the amplification factor estimated from the observed seismic intensity. It is easy to apply the station correction SC_j to EEW processing by simply substituting it for ARV, because the station correction is defined by $\mathrm{PGV}^{\mathrm{obs}}/\mathrm{PGV700}^{\mathrm{exp}}$, the same as ARV.

3. Data

3.1 Basic dataset

Seismic intensity is recorded by about 4200 seismic intensity meters installed throughout Japan by local governments, NIED, and JMA, and their data are transmitted to the JMA. JMA typically reports a seismic intensity distribution within 2–5 min after the occurrence of earthquake. Hypocentral parameters including location and M_j, called a JMA-unified catalog, are determined by JMA. The observed seismic intensities and a JMA-unified catalog for each event are compiled in the database (Ishigaki and Takagi, 2000). In this study, we used the database of events of $M_j \geq 4.0$ from May 1996 to April 2009. Focal depth and hypocentral distance were limited to shallower than 120 km and within 300 km, respectively, which is the same coverage as the dataset used in the regression analysis of the attenuation relation of Eq. (2). The earthquakes whose fault distance was estimated from the fault model are shown in Table 1. The fault models are mainly based on source inversion analysis by the Geospatial Information Authority of Japan (GSI). For those earthquakes not listed in Table 1, the fault distance was estimated using the empirical relation in Step 2 of Section 2. For M_w, we used the values determined by the NIED F-net (Okada *et al.*, 2004) moment tensor inversion (http://www.fnet.bosai.go.jp/) during or after 1997 and by the Harvard University CMT inversion (http://www.globalcmt.org/) in 1996, except for the analysis in Sections 5 and 6.

3.2 Lower limit of observed seismic intensity

A comparison of $PGV700^{exp}$ with PGV^{obs} for inland crustal earthquakes of focal depth $\leq$ 20 km is shown in Fig. 1. In this figure, we plotted only inland crustal earthquakes to avoid offsets of $PGV700^{exp}$ according to earthquake types expressed as different values of coefficient d in Eq. (2). Whereas PGV^{obs} is generally larger than $PGV700^{exp}$ because of site amplification, most of the PGV^{obs} values converted from seismic intensities less than around 2.5 are smaller than $PGV700^{exp}$. This result suggests that the empirical relation of Eq. (6) may not be applicable to low seismic intensities of less than around 2.5 or that the attenuation relation of Eq. (2) has a distance dependence for PGV^{obs}. Figure 2 shows the relationship between fault distance and the ratio of PGV^{obs} to $PGV700^{exp}$ for inland crustal earthquakes. The distribution of $PGV^{obs}/PGV700^{exp}$ for observed seismic intensities $\geq$0.5 (Fig. 2(a)) has a notable distance dependence, whereas that for intensities $\geq$2.5 (Fig. 2(b)) has little distance dependence. When distance dependence does exist, it has an inappropriate influence on the estimation of station corrections; therefore, we restricted our data to seismic intensities $\geq$2.5. Figure 3 shows the relationship between M_w and $PGV^{obs}/PGV700^{exp}$ for the same data used in Fig. 2(b). The distribution of $PGV^{obs}/PGV700^{exp}$ has little dependence on M_w.

If we estimate the station corrections from $PGV^{obs}/PGV700^{exp}$, including the data from stations at large distances from the fault, the station corrections of the latter may be larger than the real values. Therefore, we excluded the data of larger fault distances at sites at which observed seismic intensity is $<$2.5 (Fig. 4). We used earthquakes that had at least five seismic intensity observations.

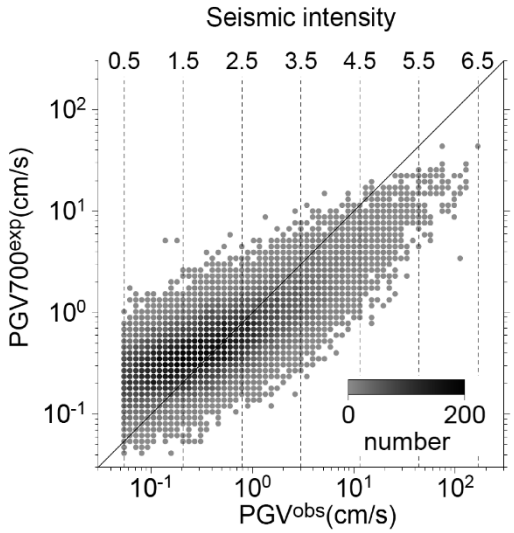

Fig. 1. Comparison of $PGV700^{exp}$ and PGV^{obs} for inland crustal earthquakes of focal depth $\leq$20 km. M_w is used for M. Observed seismic intensities (JMA intensities) correspond to the values of PGV^{obs} converted by Eq. (6).

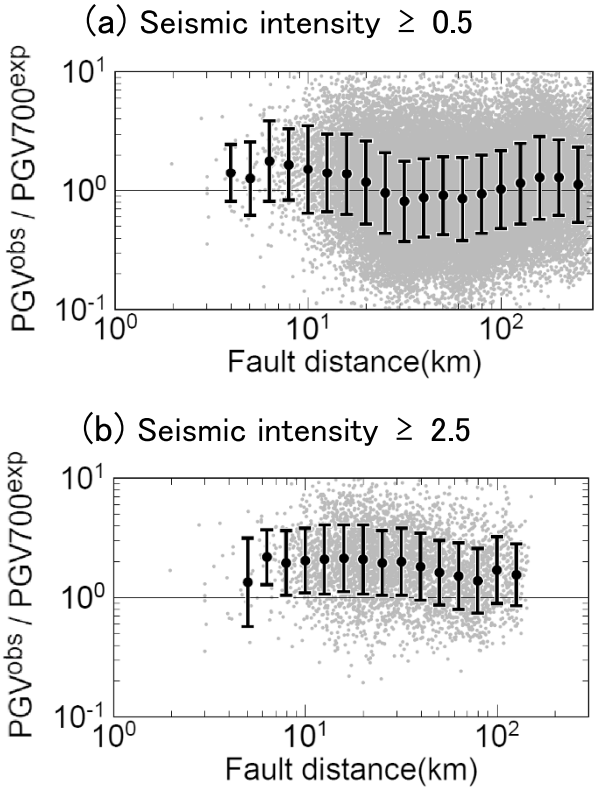

Fig. 2. Relationship between fault distance and $PGV^{obs}/PGV700^{exp}$ for inland crustal earthquakes of (a) seismic intensity $\geq$0.5 and (b) seismic intensity $\geq$2.5. M_w is used for M. Circles and bars show the average of $\log(PGV^{obs}/PGV700^{exp})$ and its standard deviation in each distance segment, respectively.

3.3 Distribution of data

The distribution of earthquakes is shown in Fig. 5, and the distribution of the data with respect to fault distance X

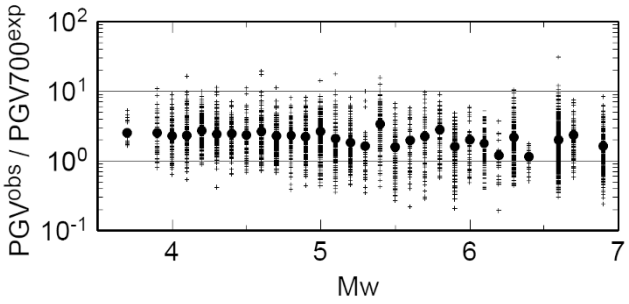

Fig. 3. Relationship between M_w and $PGV^{obs}/PGV700^{exp}$ for inland crustal earthquakes of seismic intensity $\geq$2.5. M_w is used for M. The solid circles indicate the average of $\log(PGV^{obs}/PGV700^{exp})$ at each M_w.

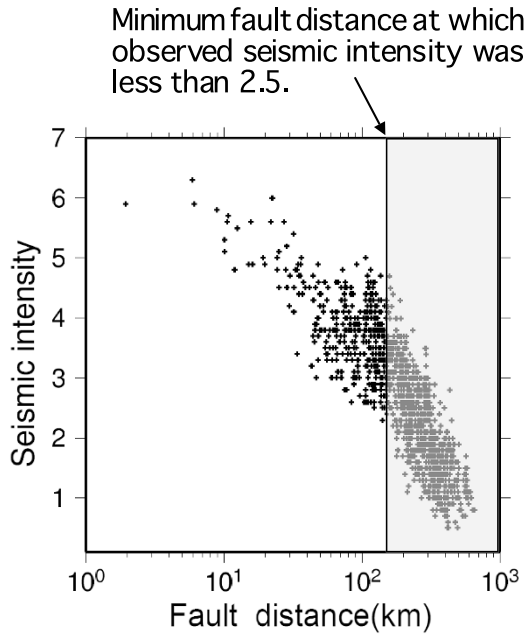

Fig. 4. Fault distance range used for the analysis. Observed seismic intensities were used from stations for which the fault distance is less than the distance of the station at which observed seismic intensity was <2.5. Data of gray area are excluded in this analysis.

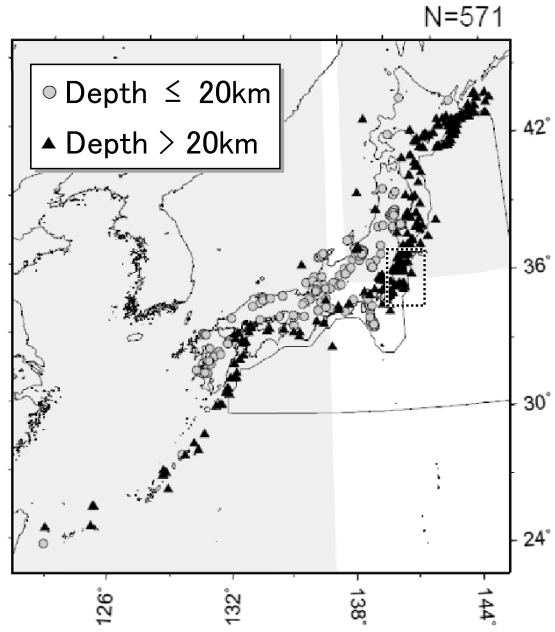

Fig. 5. Epicenters of earthquakes used in estimating station corrections for all dataset. The offshore area enclosed by the line is where focal depths >10 km are shifted to 10 km. The dotted rectangle indicates the area shown in Fig. 7. The gray areas indicate the regions where the correction term of abnormal seismic intensity distribution is applied.

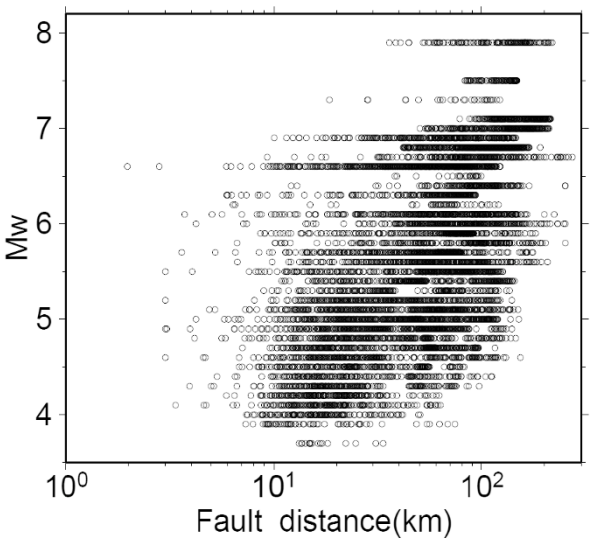

Fig. 6. Distribution of the data with respect to fault distance and M_w when estimating station corrections for all datasets.

and M_w is shown in Fig. 6. In these figures, when M_w is not reported in F-net nor in the Harvard University CMT, M_j is used. These data were used for estimating the station corrections. Although seismic intensities were compiled within a hypocentral distance of 300 km, for most data the fault distance was within about 150 km because we discarded seismic intensities of <2.5. For most offshore earthquakes far from the inland seismic observation network, the determined focal depth tends to be deeper than the seismogenic-zone because of the incomplete azimuthal coverage of the network in the JMA-unified catalog. Figure 7 shows hypocenter distribution (Aketagawa *et al.*, 2010) in the area indicated in Fig. 5. Although the focal depth of the earthquake (M_j 7.0) marked with a star in Fig. 7 is 51 km in the JMA-unified catalog, this depth is too deep compared with the plate boundary. Such earthquakes result in an overestimation of $PGV700^{exp}$. Thus, in the offshore area bounded by the line in Fig. 5, focal depths >10 km were shifted to 10 km. This area is the same as the area where focal depths are fixed at 10 km when M is estimated in the JMA EEW algorithm. When the fault distance is 150 km from the earthquake (M_j 7.0; marked with a star in Fig. 7), the $PGV700^{exp}$ increases by 1.35-fold due to the shift in the focal depth from 51 km to 10 km.

4. Estimation of Station Correction

4.1 Correction of abnormal seismic intensity distribution

An abnormal seismic intensity distribution (Utsu, 2001) is commonly observed for deep earthquakes at subduction near Japan. As shown in Fig. 8(a), an abnormal seismic in-

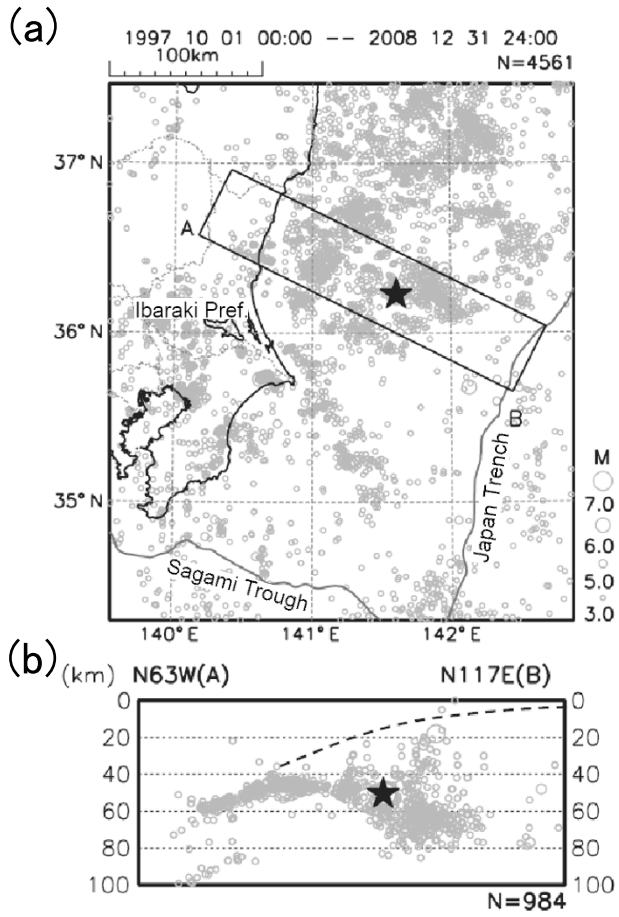

Fig. 7. Hypocenters of earthquakes in the dotted rectangle indicated in Fig. 5 (modified from Aketagawa *et al.* (2010)). (a) Epicenters of earthquakes. A star indicates the M_j 7.0 earthquake in Far East Off Ibaraki Prefecture on May 2008. (b) Vertical cross section of earthquakes along the A–B line in rectangle in (a). Dotted line indicates the plate boundary drawn from trench axis to upper boundary of slab.

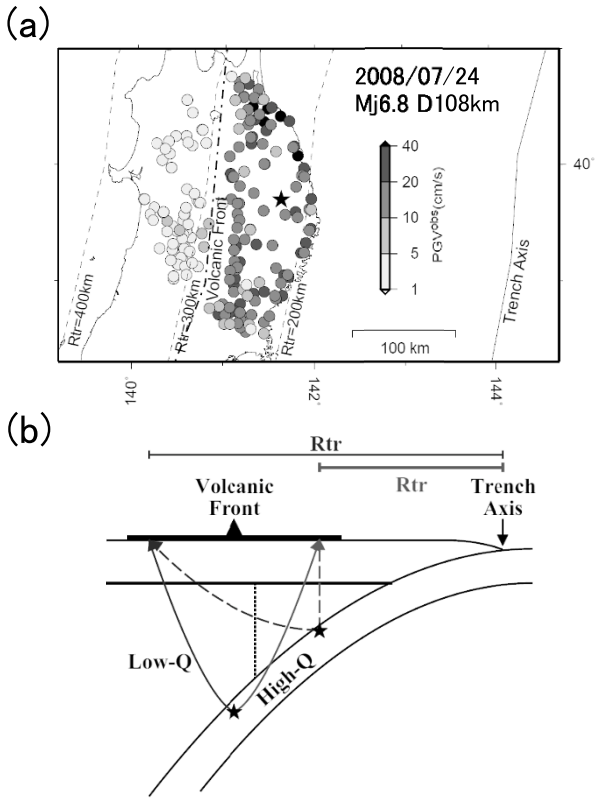

Fig. 8. (a) Example of the abnormal seismic intensity distribution in Tohoku district of Japan. A star indicates the epicenter of the intra-plate earthquake (M_j 6.8, Depth 108 km). Dotted lines indicate equidistant lines from the trench axis. Dashed-dotted line indicates volcanic front. (b) Schematic view of vertical cross section perpendicular to the trench axis for Q structure at subduction (Morikawa *et al.* (2003)). Stars indicate hypocenters. Arrows indicate ray paths from deep earthquakes to stations.

tensity distribution for deep earthquakes is a phenomenon in which strong motions in the fore-arc (east of volcanic front) are larger than those in the back-arc (west of volcanic front) are observed. This abnormal distribution is due to the effect produced by regional differences in seismic wave attenuation (Q) structure (shown in Fig. 8(b)) and cannot be explained by the effect of site or source. Here, seismic ray paths in the low-Q mantle wedge from intra-slab earthquakes to back-arc stations are longer than those to fore-arc stations. In Eq. (2), the effect of inhomogeneous Q structure is not included. In order to accommodate this abnormal distribution, additional correction terms (Morikawa *et al.*, 2003; Fujiwara *et al.*, 2009; Headquarters for Earthquake Research Promotion, 2009) were proposed for Eq. (2), H and H':

$$\log H = (-4.021\times10^{-5}\times R_{\rm tr}+9.905\times10^{-3})\times(D-30) \quad (8)$$

$$\log H' = \begin{cases} 4.28+10^{-5}\times R_{\rm vf}\times(D-30) & (R_{\rm vf}\le 75\,{\rm km}) \\ 3.21\times10^{-3}\times(D-30) & (R_{\rm vf}>75\,{\rm km}) \end{cases}, \quad (9)$$

where $R_{\rm tr}$ is the shortest distance (km) from the seismic intensity station to the Japan and Kuril trench axes, $R_{\rm vf}$ is the shortest distance (km) from the seismic intensity station to the volcanic front, and D is focal depth (km). We applied the correction terms H and H' in Eq. (2). H is multiplied by PGV700$^{\rm exp}$ for Pacific intra-slab earthquakes north of latitude 36°N and east of longitude 138°E, and H' is multiplied by PGV700$^{\rm exp}$ for Philippine Sea intra-slab earthquakes west of longitude 137°E. The areas to which these correction terms were applied are shown in Fig. 5. Figure 9(a) shows the relationship between the shortest distance from seismic intensity stations to the Japan and Kuril trench axes and PGV$^{\rm obs}$/PGV700$^{\rm exp}$ without the correction terms for earthquakes deeper than 30 km in northeastern Japan. For events most distant from the trench, PGV$^{\rm obs}$/PGV700$^{\rm exp}$ tends to be smaller in the back-arc beyond the volcanic front than in the fore-arc. The distribution of PGV$^{\rm obs}$/PGV700$^{\rm exp}$ shown in Fig. 9(a) suggests that PGV700$^{\rm exp}$ does not appropriately produce the abnormal seismic intensity distribution. Figure 9(b) shows the data of Fig. 9(a) after the correction terms, PGV$^{\rm obs}$/(PGV700$^{\rm exp}\cdot H$) have been applied. The values in Fig. 9(b) are larger than those in Fig. 9(a) for events >300 km from the trench axis. Thus, we believe that the abnormal seismic intensity distribution is adequately corrected.

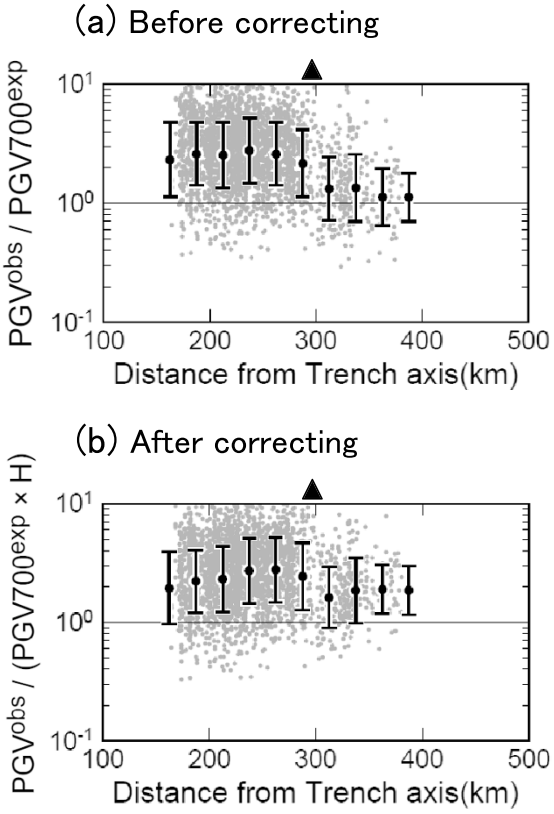

Fig. 9. Relationship between distance from seismic intensity stations to the Japan and Kuril trench axes and $PGV^{obs}/PGV700^{exp}$ for earthquakes deeper than 30 km in northeastern Japan (a) before and (b) after application of correction term H for abnormal seismic intensity distribution to $PGV700^{exp}$. M_w is used for M. Solid triangles indicate the location of the volcanic front.

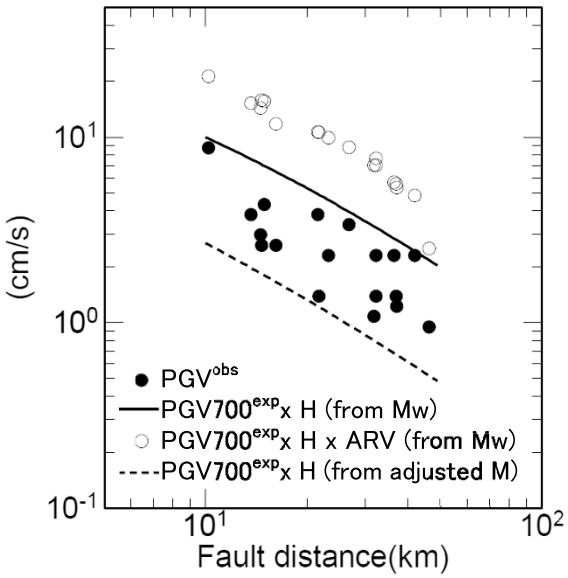

Fig. 10. Example of the inter-event variance for No. 5 earthquake listed in Table 1.

4.2 Correction of source term

The variance of an attenuation relation includes intra- and inter-event variances (Youngs *et al.*, 1995). The inter-event variance represents the difference in the strong motion between the common attenuation relation (e.g., Eq. (2)) and the attenuation relation best fitted for observations from an earthquake. Figure 10 shows an example of an earthquake (No. 5 in Table 1) included in the large inter-event variance. Whereas PGV^{obs} should be generally larger than $PGV700^{exp} \cdot H$ because of site amplification, all of PGV^{obs} (solid circle) in Fig. 10 are smaller than $PGV700^{exp} \cdot H$ (solid line). The difference in strong motion between the attenuation relation of observations PGV^{obs} and that of expectations $PGV700^{exp} \cdot H$ represents the inter-event variance. The earthquake in Fig. 10 has the largest inter-event variance in the earthquakes listed in Table 1. The main reason for the inter-event variance is that source factor M does not necessarily correspond to the stress drop affecting the seismic wave amplitude excited from the source (Midorikawa and Ohtake, 2003). Thus, the difference between PGV^{obs} and $PGV700^{exp} \cdot H$ involves not only the site amplification factor, but also the source factor. Because the station correction estimated by Eq. (7) should correspond to the site amplification factor, it should not be contaminated by the source factor expressed as an inter-event variance. We then adjusted M used in the attenuation relation to reduce the inter-event variance and also the variance caused by the difference in strong motion from different earthquake types (inter-plate earthquake, intra-slab earthquake, or crustal earthquake; Si and Midorikawa (1999)).We adjusted M to minimize

$$\text{misfit} = \sum^{N_i} \left[\log(PGV_{ij}^{obs}) - \log(PGV700_{ij}^{exp} \cdot H_{ij} \cdot ARV_j) \right]^2, \quad (10)$$

where N_i is the number of observed data for the i-th earthquake, H_{ij} is the correction term for the abnormal seismic intensity distribution described in Section 4.1, and ARV_j is ARV at the j-th observed station. The reason why $PGV700^{exp}$ is multiplied by ARV_j in Eq. (10) is to remove the effect of site amplification from the adjusted M value because the station correction is defined as the amplification factor relative to the upper engineering bedrock, as with ARV. As shown in Fig. 10, this process treats M as a free parameter when the attenuation relation of $PGV700^{exp} \cdot H \cdot ARV$ (open circle) is estimated to fit well with the attenuation relation of PGV^{obs} (solid circle), which corresponds to determining $PGV700^{exp} \cdot H$ (dotted line) from the most probable value of M. The adjusted value of M is used in estimating $PGV700^{exp}$ when we estimate the station correction.

Coefficient d in Eq. (2) represents the offset value of different earthquake types. The value of d for an intra-slab earthquake, 0.12, is much larger than the values for inland crustal and inter-plate earthquakes. Si and Midorikawa (1999) considered that the larger ground motion of intra-slab earthquakes is caused by a high stress drop at the source. Asano *et al.* (2004) showed that stress drops on the asperities of shallow intra-slab earthquakes that generate strong ground motions are higher than those of inland crustal earthquakes. To reduce the difference in $PGV700^{exp}$ caused by different earthquake types, an offset correction is needed for the attenuation relation. For those earthquakes much deeper than the plate boundary, such as a focal depth >80 km, we can identify the earthquake type as the intra-

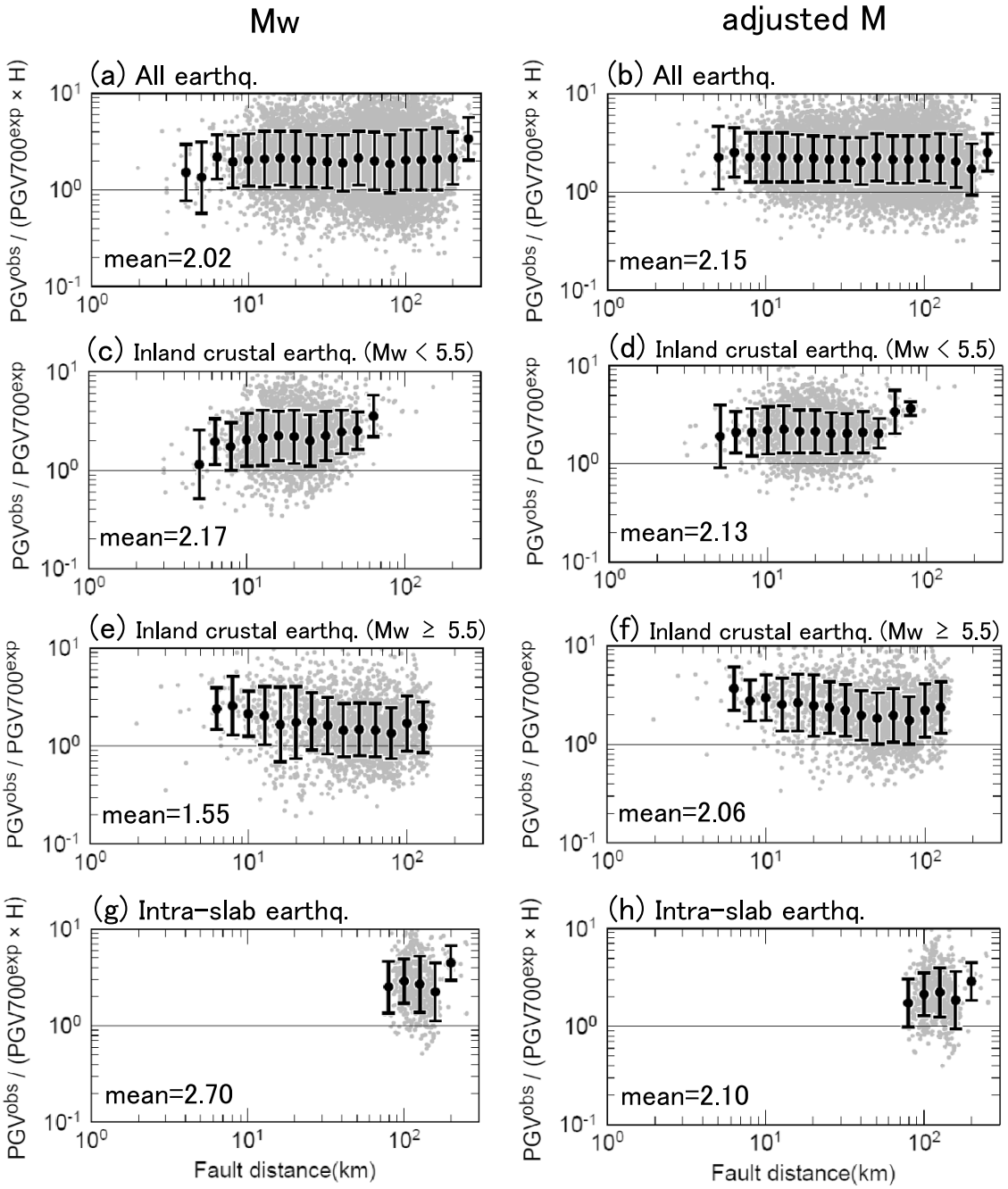

Fig. 11. Relationship between fault distance and $PGV^{obs}/PGV700^{exp}$ estimated from (left) M_w and (right) the adjusted M. (a, b) All earthquake types, (c, d) inland crustal earthquakes (depth $\leq$ 20 km) of $M_w < 5.5$, (e, f) inland crustal earthquakes (depth $\leq$ 20 km) of $M_w \geq 5.5$, (g, h) intra-slab earthquakes (depth $\geq$ 80 km). "Mean" in each panel is geometric mean of $PGV^{obs}/PGV700^{exp}$.

slab without focal mechanism, and we can also easily identify the earthquakes shallower than about 30 km far away from plate boundary as the crustal earthquakes. It is, however, difficult to identify the earthquake types for shallow earthquakes near the plate boundary. We assumed, therefore, that the adjustment of M using Eq. (10) not only reduces the inter-event variance but also has virtually the same effect as the offset correction of different earthquake types.

Figure 11 shows the relationships between fault distance and $PGV^{obs}/PGV700^{exp}$ estimated from M_w and the adjusted M. The total variance of $PGV^{obs}/PGV700^{exp}$ was reduced in all ranges of fault distance by the adjusted M (Figs. 11(a, b)). For inland crustal earthquakes, the distance dependence of $PGV^{obs}/PGV700^{exp}$ for $M_w < 5.5$ (Fig. 11(c)) was resolved by the use of adjusted M (Fig. 11(d)), but remained for $M_w \geq 5.5$ (Figs. 11(e, f)). This suggests that the correction of inter-event variance is effective, at least for small inland crustal earthquakes. Values of $PGV^{obs}/PGV700^{exp}$ near the fault for inland crustal earthquakes were relatively large, as shown in Fig. 11(f), causing overestimates of the station correction, an effect we address in Section 7. The geometric mean of $PGV^{obs}/PGV700^{exp}$ estimated from the adjusted M for intra-slab earthquakes (Fig. 11(h)) was almost the same as that for inland crustal earthquakes (Figs. 11(d,

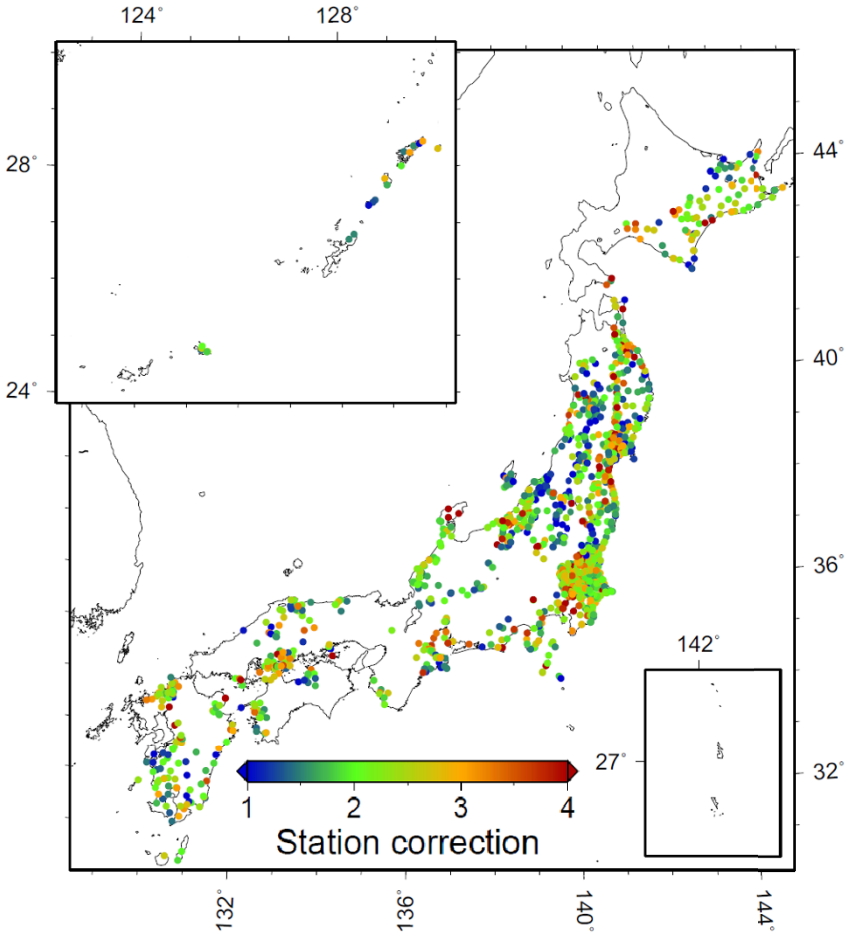

Fig. 12. Map showing spatial distribution of stations for which station corrections were obtained for all datasets.

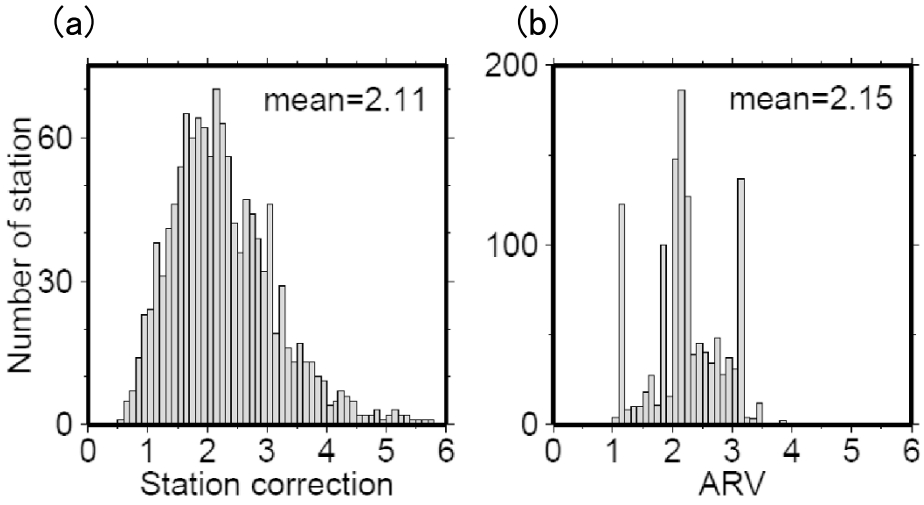

Fig. 13. Histogram of (a) station corrections and (b) ARV of stations where the station correction was obtained. "Mean" in each panel is geometric mean.

f)). In addition, for intra-slab earthquakes shown in Figs. 11(g, h), the logarithmic ratio of the geometric mean of $PGV^{obs}/PGV700^{exp}$ values for M_w and adjusted M, that is $\log(2.70/2.10) = 0.11$, was about the same as the coefficient d (0.12) in Eq. (2). These results provide a basis for assuming that adjusting M is a proper offset correction for intra-slab earthquakes.

5. Characteristics of Station Corrections

We estimated station corrections after applying the correction for abnormal seismic intensity distribution and adjusting M as previously described. The station corrections were extracted on the conditions that the station has at least three earthquake records when estimating station corrections using Eq. (7). When the standard deviation of the

common logarithm is ≥0.3, the station correction is discarded. Station corrections were obtained for all datasets for 1258 stations, about 30% of all stations in the national network (Fig. 12). Most of these are distributed near regions of earthquake occurrence. Station corrections in sedimentary basins are generally relatively large.

As shown in Fig. 13, station corrections show a smooth distribution, with a peak at their average value, whereas ARV has peaks not only at its average but also around 1 and 3. The topographic data of ARV around 1 and 3 correspond to the Pre-Neocene and the delta back marsh, respectively. The reason for the peak of ARV around 1 is that most of the topographic data on Japan's landmass are classified as Pre-Neocene. The reason for the peak of ARV around 3 is that seismic intensity meters are densely installed in populated areas where the topographies are often classified as the delta back marsh. In Fig. 14 there is a poor correlation between station corrections and the site amplification based on topographic data (the correlation coefficient is 0.30).

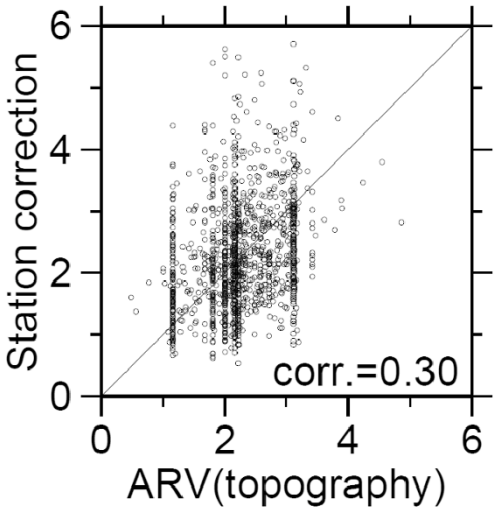

Fig. 14. Correlation between station corrections and ARV.

6. Accuracy of Expected Seismic Intensity

We computed expected seismic intensities using the method of the JMA for the EEW by using both station corrections and ARV. We split the dataset into two groups: group A, from May 1996 to December 2004; group B, from January 2005 to April 2009. We determined station corrections from group A and expected seismic intensities for group B. Note that the dataset used for the expectation of seismic intensities is independent of the dataset used for determining the station correction. We used earthquakes of $M_j \geq 4.0$ and focal depth ≤120 km and stations of observed seismic intensity ≥3.5 (Fig. 15) for the expected intensities. The expectation error was evaluated for stations where the station correction was obtained. Note that, for the evaluation of the expectation error, correction of the source term described in Section 4.2 was not applied.

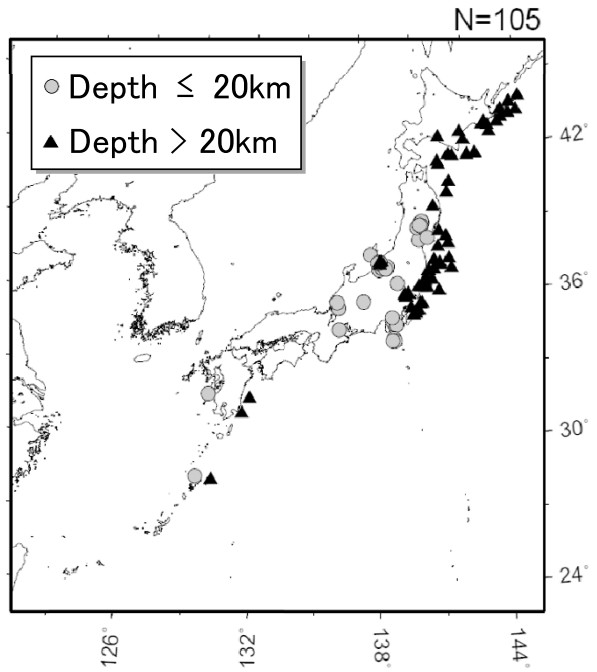

Fig. 15. Epicenters of earthquakes for which expected seismic intensities were computed for the period January 2005 to April 2009.

Figure 16 shows the distribution of seismic intensity residuals. The effect of station correction (Fig. 16(a)) was to reduce the average of residuals from 0.25 to 0.19 and to reduce the standard deviation of residuals from 0.63 to 0.55. Also, by using station correction, the number of residuals within ±1.0 was increased from 84 to 93% of the total number, and the number of residuals within ±0.5 was increased from 55 to 59% of the total number of stations.

Figure 17 compares the expectation errors estimated with station corrections and with ARV. In Fig. 17(a), the root mean square (RMS) errors for most earthquakes across the whole range of fault distances were improved by station correction, although some relatively large RMS errors occurred with station correction at some near fault distance ranges, as shown in Fig. 17(b). The RMS error for the total residual was reduced from 0.68 to 0.58, as shown in Fig. 17(a), which corresponds to a demonstration that using station correction can reduce the expectation error by 15%.

7. Discussion

In the previous section, we demonstrated that simply the replacement of ARV by empirically estimated station corrections leads to an improvement in the accuracy of expected seismic intensities for the current JMA EEW, even when other empirical relations (Eqs. (1), (2), (3), (4), and (6)) are unchanged. In addition to the improvement of site factors, it is expected that the modification of other empirical relations will lead to an improvement in accuracy. In this section, we discuss the improvement in the accuracy of expected seismic intensities through enhancement of the other empirical relations.

In this study, we focus on the improvement of accuracy of expected seismic intensities for the current JMA EEW through replacing ARV by empirically estimated station correction, even when other empirical relations (Eqs. (1), (2), (3), (4) and (6)) are not changed. Therefore, the station correction was estimated using the same empirical relations that underlie the JMA EEW's logic. In addition, when estimating station corrections, we applied corrections of the

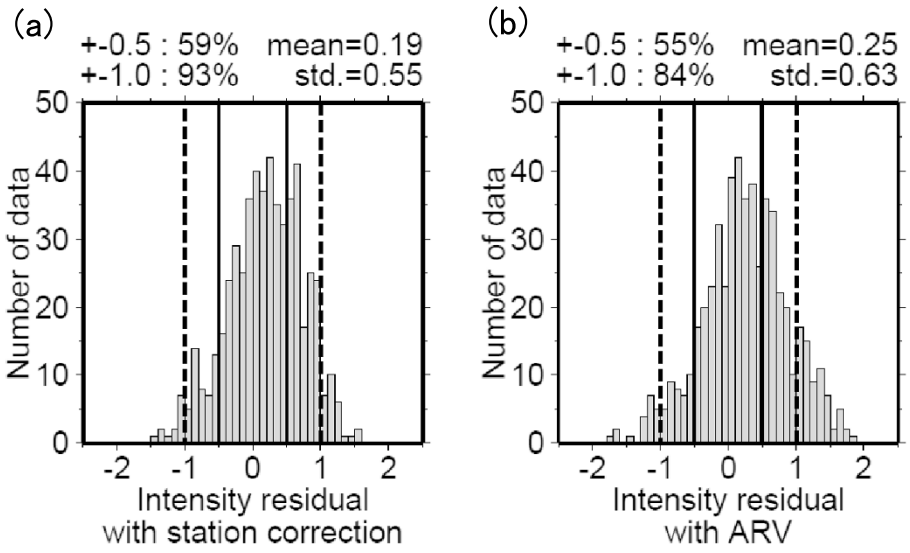

Fig. 16. Histogram of seismic intensity residuals estimated with (a) station correction and with (b) ARV within ±0.5 and ±1.0 residuals shown by solid and dotted lines, respectively.

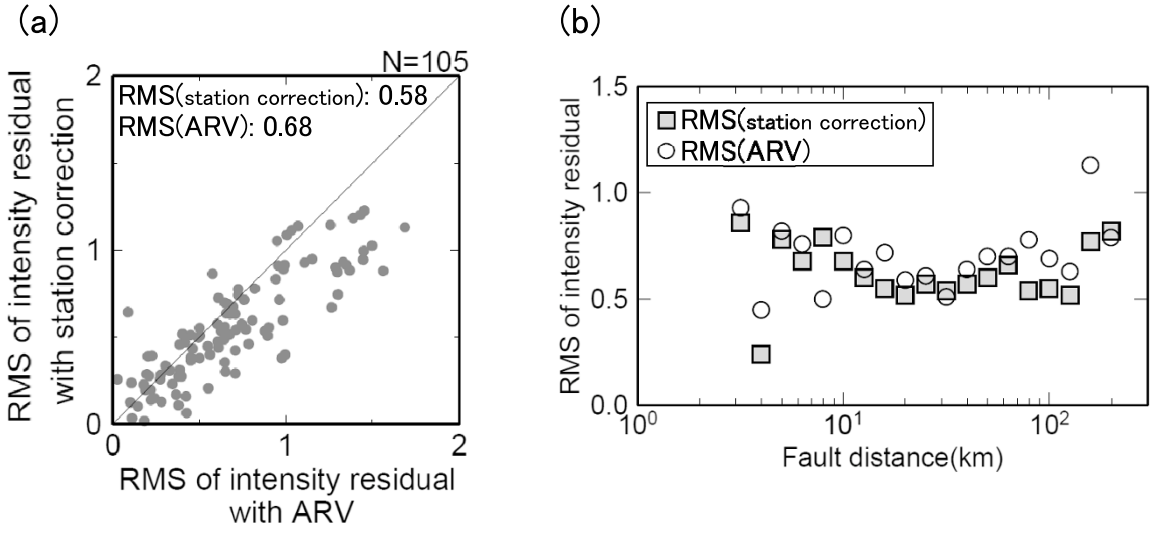

Fig. 17. Comparison of RMS seismic intensity residuals estimated with station correction and with ARV for (a) individual earthquakes and (b) the average of RMS in each distance segment. Upper left values in (a) indicate total RMS. Squares and circles in (b) indicate RMS with station correction and ARV, respectively.

abnormal seismic intensity distribution and source term for Eq. (2) in order to reduce the effects of factors other than site amplification. As a result, the error in expected seismic intensity was improved using our station correction. However, when estimating station corrections, we had to limit observed seismic intensities to those $\geq$2.5, mainly to reduce the distance dependence of $PGV^{obs}/PGV700^{exp}$. To reduce these residuals between the empirical relations and observed data, a new empirical relation should be regressed from recently observed data. Iwakiri *et al*. (2009) suggested that the attenuation relation of seismic intensity with M_j (Matsusaki *et al*., 2006) showed no dependence on fault distance within 100 km for recently observed data. In the future, when such a new empirical relation is introduced in the JMA EEW, it would therefore be possible to improve the accuracy of the expected seismic intensities. When estimating the station correction, we adjusted M by using observed seismic intensity to reduce the variance of the attenuation relation as described in Section 4. However, in the current JMA EEW algorithm, M is not estimated by using observed seismic intensity. Yamamoto *et al*. (2008) proposed using the observed seismic intensity itself to estimate M and showed that this method reduced the errors of estimated seismic intensities compared with use of M_j. In the JMA EEW algorithm, the accuracy of expected seismic intensity may be improved if M is estimated by observed seismic intensity.

Fujiwara *et al*. (2007) showed that the site amplification based on topographic data correlates weakly with the empirical site amplification estimated from the attenuation relation of K-NET (strong motion network operated by NIED). In Fig. 14, it is also shown that the correlation between our station corrections at the stations and the site amplification based on topographic data is weak. The errors of expected

seismic intensity with ARV were improved by station corrections for most earthquakes. These may suggest that ARV does not always represent site amplification just under the station, as the topographic data are represented by a 1-km square mesh cell. It may also be that ARV contains uncertainty stemming from the relation between AVS and ARV used in estimating ARV from topographic data.

As shown in Fig. 11(f), we found relatively large strong motions near the fault. One of the possible reasons for this is that strong motions observed near the fault may arise from factors in addition to site amplification. Midorikawa (2009) proposed that large strong motion variations near faults for recent inland crust earthquakes are caused by fault rupture propagation effects or the heterogeneous distribution of asperities. For example, observed seismic intensities for the 2004 Mid Niigata earthquake were relatively high on the hanging-wall side of the reverse fault (Midorikawa, 2006) and can be explained by the hanging-wall effect (Abrahamson and Somerville, 1996). If we clearly find that strong motions observed near faults show a misfit to the attenuation relation for any other reason than site amplification, these data should not be used for estimation of the station corrections. However, it is sometimes difficult to identify whether the reason for the misfit of each earthquake is site amplification or not. It is also hard to fix the range of fault distance corresponding to misfit for each earthquake. Thus, we do not limit the range of fault distance near the fault when adjusting M and estimating the station corrections.

Kiyomoto *et al.* (2010) estimated site factors using observed seismic intensities $\geq$3.5 with the attenuation relation of Eq. (2). These researchers also conclude that replacing ARV by empirically estimated site factors improves the accuracy of seismic intensity expectation. The difference between our calculations and those of Kiyomoto *et al.* (2010) is that we reduced the uncertainty of station corrections by introducing the adjustment of M and the correction of abnormal seismic intensity distribution; we also raised the number of stations where station corrections are estimated by using an observed seismic intensity of $\geq$2.5.

Hoshiba *et al.* (2010) showed that even when the path factor and site amplification factor are appropriately evaluated, the uncertainty is expected to be 0.29 units on the JMA intensity scale if M_{j} is used as the index of the source factor, which is the intrinsic uncertainty limit for expected seismic intensity in the current JMA EEW algorithm. The expectation error in this study was 0.58 intensity units even when the station correction was used as the site amplification factor. Such a large expectation error would be due to the variance of attenuation and other empirical relations when estimating station corrections and expecting seismic intensities.

For present seismic intensity expectation of the JMA EEW, the effect of soil non-linearity is not included. The soil non-linearity during strong motion appears at more than about 15 cm/s of PGV (Midorikawa, 1993). On the other hand, the soil non-linearity on PGV is very small compared with peak ground acceleration (Midorikawa and Ohtake, 2003; Fujimoto and Midorikawa, 2006). Our station correction does not include the soil non-linearity. In the future, when we consider the soil non-linearity for large PGV, our station correction may be improved.

There has been a discussion of whether seismic intensity at each station represents typical strong motion around the area of the station. The seismic intensity itself indicates observationally the characteristic of ground motion at the station only (information of the point), but it is also required to be representative—to some extent—of the area around the station from a point of view of rapid estimation of possible damage to the area (representative of the area). Because of this requirement, the JMA has been surveying observed data and the installation environment to determine whether the station can be considered to be a properly representative observation site of the area (JMA, and Fire and Disaster Management Agency, 2009). When the station is identified as an inappropriate site, the seismic intensity meter is moved to another site or is not longer used as an observation site (when it is moved, new station ID is applied). In this paper, we discussed the improvement in the expectation of seismic intensity by replacing ARV by an empirically estimated station correction. Our purpose is to improve seismic intensity expectation at the locations installed seismic intensity meters. This improvement may be applicable only at the observational sites, but our analysis suggests that the expectation of ground motion in the EEW can be improved at locations where a seismic observation has been made, as compared with the locations where only topographic data are available.

8. Conclusions

To identify a more accurate solution for site effects than that provided by the site amplification factor ARV based on topographic data in the JMA EEW algorithm, we estimated station corrections by comparing the attenuation relation with observed seismic intensities from recent earthquakes. We applied a correction for the abnormal seismic intensity distribution and the adjustment of M. Station corrections for 1258 stations were obtained, which is about 30% of the national seismic intensity network. The correlation between station corrections and the site amplification based on topographic data is weak. The RMS accuracy of expected seismic intensities for the most recent 4 years was improved by 15% by using station corrections estimated from data of the previous 8 years, which means that the simple replacement of ARV by empirically estimated station corrections leads to an improvement in seismic intensity expectation even when other empirically relations (Eqs. (1), (2), (3), (4), and (6)) remain unchanged. Relatively large RMS errors in the station correction, however, persist near faults, which are probably explained not only by site amplification factor but also by fault rupture effects.

Acknowledgments. We are grateful to Dr. Maren Boese and an anonymous reviewer for their valuable comments and suggestions. We also thank the editor Dr. Tatsuhiko Hara for his valuable comments. Our seismic intensity dataset was recorded at seismic intensity meters operated by local governments, NIED, and JMA. For hypocentral information we used the JMA seismic catalog unified seismic data from NIED, Hokkaido University, Hirosaki University, Tohoku University, University of Tokyo, Nagoya University, Kyoto University, Kochi University, Kyushu

University, Kagoshima University, the National Institute of Advanced Industrial Science and Technology, the Tokyo Metropolitan Government, the Shizuoka Prefectural Government, the Kanagawa Prefectural Government, the City of Yokohama, the Japan Marine Science and Technology Center, and JMA. Figures were prepared using GMT (Wessel and Smith, 1991).

References

Abrahamson, N. A. and P. G. Somerville, Effects of hanging wall and footwall on ground motion recorded during the Northridge earthquake, *Bull. Seismol. Soc. Am.*, **86**, S93–S96, 1996.

Aketagawa, T., M. Kiyomoto, T. Shimoyama, K. Moriwaki, and T. Yokota, Improvement of P-wave magnitude estimation for Earthquake Early Warning from JMA, *Q. J. Seismol.*, **73**, 123–134, 2010 (in Japanese).

Asano, K., T. Iwata, and K. Irikura, Characterization of source models of shallow intra-slab earthquakes using strong motion data, *Proc. 13th World Conf. Earthq. Eng.*, 835, 2004.

Doi, K., The operation and performance of Earthquake Early Warnings by the Japan Meteorological Agency, *Soil Dyn. Earthq. Eng.*, 2010 (in press).

Fujimoto, K. and S. Midorikawa, Relationship between average shear-wave velocity and site amplification inferred from strong motion records at nearby station pairs, *J. Jpn. Assoc. Earthq. Eng.*, **6**(1), 11–22, 2006 (in Japanese).

Fujiwara, H., N. Morikawa, Y. Ishikawa, T. Okumura, J. Miyakoshi, and N. Nojima, Verification of the probabilistic seismic hazard maps for Japan (part 1), *Proc. 5th Ann. Meet. JAEE*, 96–97, 2007 (in Japanese).

Fujiwara, H., S. Kawai, S. Aoi, N. Morikawa, S. Senna, N. Kudo, M. Ooi, K. Hao, K. Wakamatsu, Y. Ishikawa, T. Okumura, T. Ishii, S. Matsushima, Y. Hayakawa, N. Toyama, and A. Narita, A study on "National Seismic Hazard Maps for Japan", *Technical Note of the National Research Institute for Earth Science and Disaster Prevention*, **336**, 2760 pp., 2009.

Harada, T., Earthquake versatile observation system, *Q. J. Seismol.*, **70**, 73–81, 2007 (in Japanese).

Headquarters for Earthquake Research Promotion, *Technical Report on National Seismic Hazard Maps for Japan*, 2009 (in Japanese).

Hoshiba, M., O. Kamigaichi, M. Saito, S. Tsukada, and N. Hamada, Earthquake early warning starts nationwide in Japan, *Eos Trans. AGU*, **89**, 73–74, 2008.

Hoshiba, M., K. Ohtake, K. Iwakiri, T. Aketagawa, H. Nakamura, and S. Yamamoto, How precisely can we anticipate seismic intensities? A study of uncertainty of anticipated seismic intensities forthe Earthquake Early Warning method in Japan, *Earth Planets Space*, **62**, 611–620, 2010.

Ishigaki, Y. and A. Takagi, JMA seismic intensity data base and several operational utility examples, *Q. J. Seismol.*, **63**, 75–92, 2000 (in Japanese).

Iwakiri, K., M. Hoshiba, and K. Ohtake, Study on attenuation relations focused on near source region—Evaluation of their applicability for earthquake early warning—, *Abstr. Jpn. Geosci. Union Meet. 2009*, Y230-P001, 2009.

Iwata, T. and K. Irikura, Separation of source, propagation and site effects from observed S-waves, *Zisin 2*, **39**, 579–593, 1986 (in Japanese).

Japan Meteorological Agency, *Seismic Intensity*, pp 238, Gyosei, Tokyo, 1996 (in Japanese).

Japan Meteorological Agency, Location map of seismic intensity stations in Japan, *Monthly Report on Earthquakes and Volcanoes in Japan December 2009*, 121–124, 2009 (in Japanese).

Japan Meteorological Agency, and Fire and Disaster Management Agency, Investigative commission of seismic intensity, http://www.seisvol.kishou.go.jp/eq/shindo_kentokai/index.html, 2009 (in Japanese).

Japan Meteorological Agency Seismological Volcanological Department, Technical reference for outline and processing method of earthquake early warning, http://www.seisvol.kishou.go.jp/eq/EEW/kaisetsu/Whats_EEW/reference.pdf, 2008 (in Japanese).

Kamigaichi, O., M. Saito, K. Doi, T. Matsumori, S. Tsukada, K. Takeda, T. Shimoyama, K. Nakamura, M. Kiyomoto, and Y. Watanabe, Earthquake early warning in Japan: Warning the general public and future prospects, *Seismol. Res. Let.*, **80**, 717–726, 2009.

Kikuchi, M., EIC Seismological Note, No. 5, http://www.eri.u-tokyo.ac.jp/sanchu/Seismo_Note/EIC_News/961019.html, 1996 (in Japanese).

Kikuchi, M. and K. Yamanaka, EIC Seismological Note, No. 18, http://www.eri.u-tokyo.ac.jp/sanchu/Seismo_Note/EIC_News/970326.html, 1997a (in Japanese).

Kikuchi, M. and K. Yamanaka, EIC Seismological Note, No. 22, http://www.eri.u-tokyo.ac.jp/sanchu/Seismo_Note/EIC_News/970513.html, 1997b (in Japanese).

Kikuchi, M. and K. Yamanaka, EIC Seismological Note, No. 24, http://www.eri.u-tokyo.ac.jp/sanchu/Seismo_Note/EIC_News/970625.html, 1997c (in Japanese).

Kiyomoto, M., T. Aketagawa, K. Ohtake, T. Shimbaru, T. Shimoyama, K. Moriwaki, K. Doi, and T. Yokota, Investigation of technical issues for Earthquake Early Warning, *Q. J. Seismol.*, **73**, 135–150, 2010 (in Japanese).

Matsuoka, M. and S. Midorikawa, The digital national land information and seismic microzoning, *Proceeding of the 22nd Symposium of Earthquake Ground Motion, AIJ*, 23–34, 1994 (in Japanese).

Matsusaki, S., Y. Hisada, and Y. Fukushima, Attenuation relation of JMA seismic intensity applicable to near source region, *J. Struct. Constr. Eng. AIJ*, **604**, 201–208, 2006 (in Japanese).

Midorikawa, S., Nonlinearity of site amplification during strong ground shaking, *Zisin 2*, **46**, 207–216, 1993 (in Japanese).

Midorikawa, S., Some problems related to empirical predictions of strong motion, *Bull. Earthq. Res. Inst. Univ. Tokyo*, **81**, 253–258, 2006.

Midorikawa, S., National probabilistic seismic hazard maps and future issues, *Doc. 2009 Disaster Research Forum*, 41–54, http://www.nliro.or.jp/news/2009/091120_4.pdf, 2009 (in Japanese).

Midorikawa, S. and Y. Ohtake, Empirical analysis of variance of ground motion intensity in attenuation relationships, *J. Jpn. Assoc. Earthq. Eng.*, **3**(1), 59–70, 2003 (in Japanese).

Midorikawa, S., K. Fujimoto, and I. Muramatsu, Correlation new J.M.A. instrumental seismic intensity with former J.M.A. seismic intensity and ground motion parameters, *J. Inst. Social Safe. Sci.*, **1**, 51–56, 1999 (in Japanese).

Miyamachi, H., K. Iwakiri, H. Yakiwara, K. Goto, and T. Kakuta, Fine structure of aftershock distribution of the 1997 Northwestern Kagoshima Earthquakes with a three-dimensional velocity model, *Earth Planets Space*, **51**, 233–246, 1999.

Morikawa, N., T. Kanno, A. Narita, H. Fujiwara, and Y. Fukushima, Additional correction terms for attenuation relations corresponding to the anomalous seismic intensity in Northeast Japan, *J. Jpn. Assoc. Earthq. Eng.*, **3**(4), 14–26, 2003 (in Japanese).

National Research Institute for Earth Science and Disaster Prevention, Source process inversion 2008 north coast of Iwate Prefecture by near field strong motion data, http://www.k-net.bosai.go.jp/k-net/topics/iwate_20080724/inversion, 2008 (in Japanese).

Okada,Y., K. Kasahara, S. Hori, K. Obara, S. Sekiguchi, H. Fujiwara, and A. Yamamoto, Recent progress of seismic observation networks in Japan Hi-net, F-net, K-NET and KiK-net, *Earth Planets Space*, **56**, xv–xxviii, 2004.

Si, H. and S. Midorikawa, Attenuation relationships of peak ground acceleration and velocity considering effects of fault type and site condition, *J. Struct. Constr. Eng., AIJ*, **523**, 63–70, 1999 (in Japanese).

Utsu, T., Relationships between earthquake magnitude scales, *Bull. Earthq. Res. Inst. Univ. Tokyo*, **57**, 465–497, 1982 (in Japanese).

Utsu, T., *Seismology*, 3rd ed., Kyoritsu, 376 pp., 2001 (in Japanese).

Wessel, P. and W. H. F. Smith, Free software helps map and display data, *Eos Trans. AGU*, **72**, 441, 1991.

Yamamoto, S., P. Rydelek, S. Horiuchi, and C. Wu, On the estimation of seismic intensity in earthquake early warning systems, *Geophys. Res. Lett.*, **35**, L07302, doi:10.1029/2007GL033034, 2008.

Yamanaka, K. EIC Seismological Note, No. 141, http://www.eri.u-tokyo.ac.jp/sanchu/Seismo_Note/EIC_News/031031.html, 2003 (in Japanese).

Youngs, R. R., N. Abrahamson, F. I. Mkdisi, and K. Sadigh, Magnitude dependence variance of peak ground acceleration, *Bull. Seismol. Soc. Am.*, **85**, 1161–1176, 1995.

K. Iwakiri (e-mail: kiwakiri@mri-jma.go.jp), M. Hoshiba, K. Nakamura, and N. Morikawa